A&A 445, L9–L13 (2006)
DOI: 10.1051/0004-6361:200500217

Astronomy & Astrophysics

On the complex X-ray structure tracing the motion of Geminga

A. De Luca[1], P. A. Caraveo[1], F. Mattana[1,2], A. Pellizzoni[1], and G. F. Bignami[3,4,1]

[1] INAF – IASF, Via Bassini 15, 20133 Milano, Italy
e-mail: deluca@iasf-milano.inaf.it
[2] Università di Milano Bicocca, Dipartimento di Fisica, P.za della Scienza 3, 20126 Milano, Italy
[3] CESR/CNRS, 9 Av. du colonel Roche, 31028 Toulouse Cedex 4, France
[4] Università degli Studi di Pavia, Dipartimento di Fisica Nucleare e Teorica, via Bassi 4, 27100 Pavia, Italy

Received 17 August 2005 / Accepted 13 November 2005

ABSTRACT

A deep (100 ks) XMM-Newton observation of Geminga has shown two faint tails of diffuse X-ray emission, extending for ∼2′ behind the pulsar, well aligned with the proper motion (PM) direction. We report here on a recent ∼20 ks Chandra observation, which unveils a new structure, ∼25″ long and ∼5″ thick, starting at the pulsar position and perfectly aligned with the PM direction, with a surface brightness ∼40 times higher than that of the XMM Tails. The Chandra comet-like feature has a remarkably hard spectrum (photon index ∼0.9−1.4) and a luminosity of $\sim 5.5 \times 10^{28}$ erg s^{-1}, comparable to the energetics of the larger XMM one. Geminga is thus the first neutron star to show a clear X-ray evidence of a large-scale, outer bow-shock as well as a short, inner cometary trail.

Key words. stars: neutron – pulsars: individual: Geminga – X-rays: stars

1. Introduction

Isolated Neutron Stars (INSs) inherit high space velocities from their supernova explosions. Moreover, INSs are known to be efficient particle accelerators. They power a particle wind which is supposed to account for the bulk of their observed rotational energy loss ($\dot{E}_{\rm rot}$). When the particle wind from a fast moving INS interacts with the surrounding Interstellar Medium (ISM), it gives rise to complex structures, globally named "Pulsar Wind Nebulae" (PWNe) where $\sim 10^{-5}$–10^{-3} of the INS $\dot{E}_{\rm rot}$ is converted into electromagnetic radiation (see Gaensler et al. 2004; Gaensler 2005, for recent reviews). The study of PWNe may therefore give insights into the geometry and energetics of the particle wind and, ultimately, the configuration of the INS magnetosphere and the mechanisms of particle acceleration. Moreover, PWNe may probe the surrounding ISM, allowing to measure its density and ionization state.

A basic classification of PWNe rests on the nature of the external pressure confining the neutron star wind (Gaensler 2005). For young INSs ($\lesssim$few 10^4 y) the pressure of the surrounding supernova ejecta plays a major role and a Crab-like PWN is formed. For older systems ($\gtrsim 10^5$ y) the INS moves through the unperturbed ISM and the wind is confined by ram pressure to form a Bow-shock PWN.

Crab-like PWNe (see Slane 2005, for a review) show usually complex morphologies, such as tori and/or jets, typically seen in X-rays. A remarkable axial symmetry, observed in several cases, is thought to trace the INS rotational axis. The alignement between the X-ray jets and the INS proper motion directions, observed for the Crab and Vela pulsars (Caraveo & Mignani 1999; Caraveo et al. 2001) implies an alignement between the rotational axis and the proper motion of the two neutron stars, with possible important implications for the understanding of supernova explosion mechanisms (Lai et al. 2001).

Bow-shocks (see Chatterjee & Cordes 2002; Gaensler 2005, for reviews) are observed around older, less energetic INSs and have a simpler, "velocity-driven" morphology. They are seen in H_α as arc-shaped structures tracing the forward shock, where the neutral ISM is suddenly excited. Alternatively, X-ray emission (and/or radio emission on larger scales) is seen to trail the INS, forming a comet-like tail, due to synchrotron radiation from the shocked INS particles diffusing downstream (only in the case of PSR B1957+20 both the H_α and the X-ray structures have been observed, Stappers et al. 2003). In X-rays, Bow shocks are typically fainter than Crab-like PWNe, favouring the detection of nearby objects.

Proximity plays a key role in the case of Geminga. A deep 100 ks observation with XMM-Newton allowed Caraveo et al. (2003) to detect two very faint patterns, or "Tails", of diffuse X-ray emission trailing the neutron star, well aligned along the proper motion direction.

Recently, the Geminga field was imaged by Chandra. In the following sections we will report on our analysis of the X-ray data, including a summary of the XMM-Newton results.

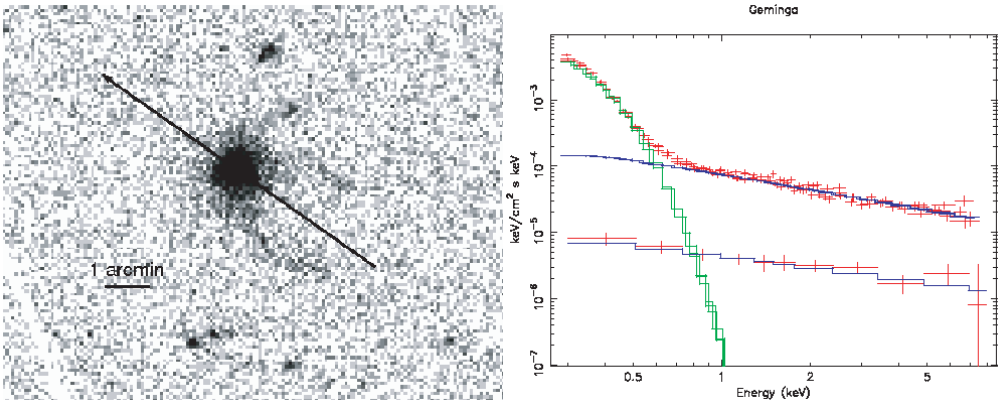

Fig. 1. *The left panel* shows the EPIC/MOS image of the inner Geminga field. Data from MOS1 and MOS2 cameras have been combined. The presence of two Tails of diffuse emission, aligned with the pulsar proper motion direction (marked by the arrow), is apparent. *The right panel* shows the unfolded spectrum of the diffuse Tails (*lower plot*) compared to the Geminga pulsar unfolded spectrum (*upper plot*). To describe the pulsar spectrum we used a double-component model (Caraveo et al. 2004), encompassing a blackbody ($T \sim 5 \times 10^5$ K, green curve), representing thermal emission from the star surface, as well as a power law (photon index 1.7 ± 0.1, blue curve), representing non-thermal emission originating in the pulsar magnetosphere. The tails' spectrum is well described by a hard power law (see text).

We will then discuss possible physical interpretations of the complex morphology of the Geminga PWN.

2. The X-ray data and their analysis

2.1. XMM-Newton observation

Geminga has been imaged on April 4th, 2002 for ∼100 ks using the EPIC instrument. The analysis of the data collected with the MOS cameras yielded the detection of a symmetric structure consisting of two tails ∼2 arcmin long trailing the pulsar, well aligned with its proper motion vector (see Fig. 1, left panel). The spectrum of both tails, extracted from the ∼2 square arcmin region where the diffuse emission is resolved from the pulsar Point Spread Function (PSF) wings, is well described by a power law with an absorption consistent with that observed for the pulsar itself, $N_{\rm H} = 1.1 \times 10^{20}$ cm^{-2} (see Caraveo et al. 2003, and references therein). Using such an $N_{\rm H}$ value, the photon index of the 450-counts tails spectrum is 1.6 ± 0.2, similar to the non-thermal component detected in the pulsar emission, also shown in Fig. 1 (right panel). The observed average surface brightness in the 0.3−5 keV range is $\sim 10^{-14}$ erg cm^{-2} s^{-1} arcmin^{-2}; the total unabsorbed flux from the region is $\sim 2.1 \times 10^{-14}$ erg cm^{-2} s^{-1}. At the 160 pc parallax distance, this translates into a 0.3−5 keV luminosity of $\sim 6.5 \times 10^{28}$ erg s^{-1}, or ∼2% of the total X-ray source luminosity in the same range, corresponding to a few 10^{-6} of Geminga's rotational energy loss.

2.2. Chandra observation

The Chandra observation of the field of Geminga started on 2004, February 7 at 13:02 UT and lasted for 19.9 ks. The Geminga pulsar was imaged on the back-illuminated S3 chip of the ACIS detector (Burke et al. 1997).

In order to reduce the pile-up at the Geminga pulsar position, the 1/8 subarray mode was used. The choice of such an operating mode yields a time resolution of 0.7 s, but limits the Field Of View (FOV) to ∼1 arcmin along the CCD readout direction.

Data were retrieved through the Chandra X-ray Centre (CXC) Archive and were processed with the CIAO software v.3.2.1, using CALDB v.3.0.1, to produce calibrated "level 2" event lists. No periods of high background were identified, for a total good exposure time of 18.7 ks. In our analysis we used only events from the ACIS-S3 chip in the 0.45−7 keV range.

The resulting ACIS image, zoomed on the Geminga position, is shown in Fig. 2 (left panel) at its full resolution (pixel size of ∼0.5 arcsec). In the middle panel of the same figure, the ACIS image, rebinned to a pixel size of ∼2″, has been superimposed to the XMM-Newton MOS 0.3−8 keV image.

The Geminga pulsar is clearly detected by Chandra with a count rate of 7.1 ± 0.2 × 10^{-2} counts s^{-1} (0.45−7 keV, extraction region of 3″ diameter) and a spectrum consistent (within the limited statistics) with the results from XMM-Newton (Caraveo et al. 2004). The source coordinates ($\alpha = 06^{\rm h}33^{\rm m}54.21^{\rm s}$, $\delta = 17°46'14.2''$) are within ∼0.7″ from the values expected on the basis of the source absolute optical position and proper motion (Caraveo et al. 1996, 1998). A faint pattern of diffuse emission, with a length of ∼25″ and a width of ∼5″, is also seen to trail the pulsar, perfectly aligned with the neutron star proper motion direction. We shall refer to such feature as the "Chandra Trail", while the diffuse emission detected by XMM-Newton will remain the "XMM Tails".

The brightness profile of the Chandra Trail along the direction of the pulsar proper motion is shown in Fig. 3, where each bin corresponds to the counts in a rectangular area 3″ long in the PM direction and 7″ wide perpendicular to it (see inset of Fig. 3); the background level was evaluated from a 60″ × 90″ region North of the source region, entirely read by the same CCD node. In order to quantify the contribution from the bright pulsar in the bins immediately surrounding its centroid, an ad hoc PSF was simulated using the *ChaRT* software, following the CXC threads and using the known

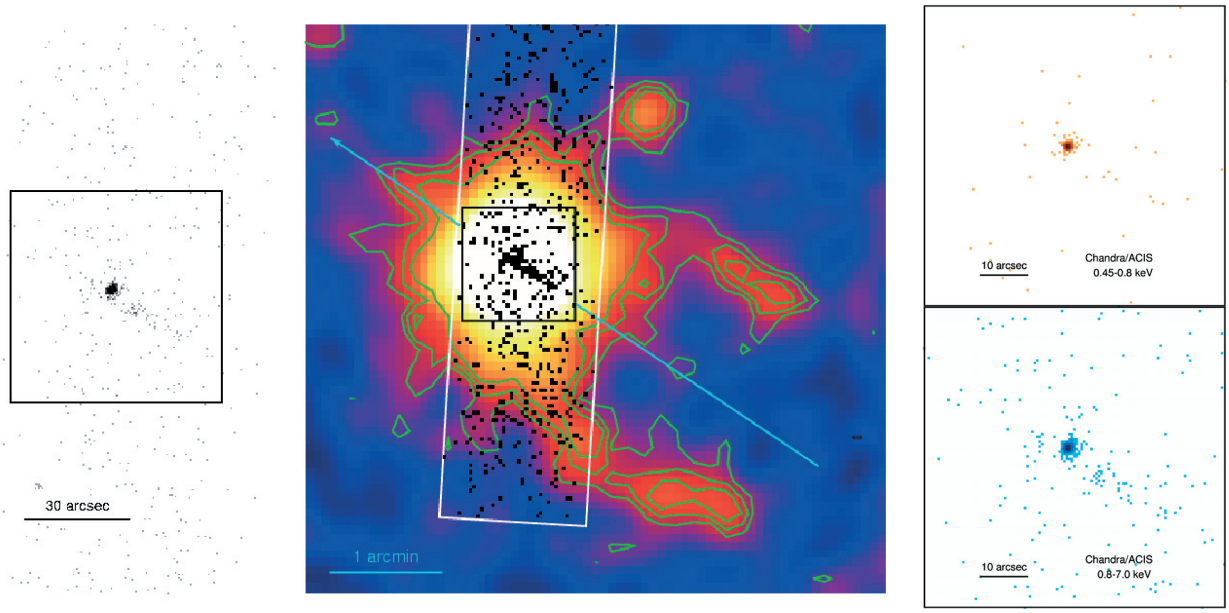

Fig. 2. The ACIS image (0.45−7 keV, 0.492″ pixel size), zoomed on the Geminga pulsar position, is shown in the *left panel*. *In the middle panel*, the same image, rebinned to a pixel size of 2″, has been superimposed on the XMM-Newton/MOS smoothed image. Surface brightness contours for the XMM image have been also plotted. The pulsar proper motion direction is marked by an arrow. The ACIS field of view is marked by the white rectangular box. The black box identifies an identical 1′ × 1′ region in all panels. In the right panel, the ACIS images in the 0.45−0.8 keV and 0.8−7 keV ranges are shown. While the Chandra Trail is virtually invisible in the softer band, it appears very clearly at higher energy, pointing towards a hard spectral shape.

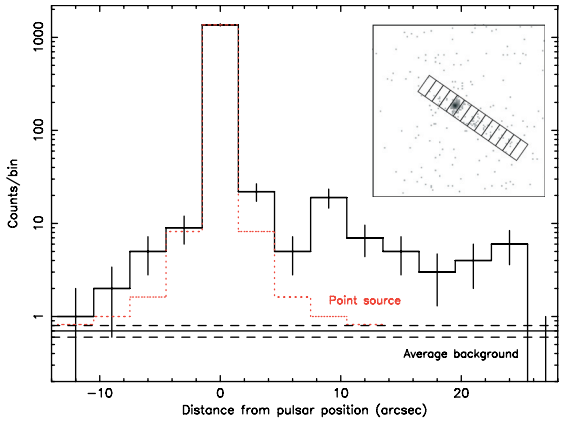

Fig. 3. Brightness profile of the diffuse Chandra Trail, computed along the pulsar proper motion direction. Each bin contains the counts detected in a 7″ × 3″ rectangular box, as shown in the inset. The region represented in the inset is the same marked by the black box in Fig. 2.

spectrum of Geminga. The estimated profile of the point source within the histogram bins has been plotted in Fig. 3 as a dotted line. Although a mild pile-up is possibly distorting a little the actual PSF, Fig. 3 suggests that no significant diffuse emission is detected ahead of the pulsar. Behind the pulsar, the Chandra Trail extends along the proper motion direction up to a distance of ∼25″, close to the limit of the instrument FOV. Considering a trail region 22″ long and 7″ thick extending behind Geminga, and neglecting the region within 4.5″ of the pulsar, a total (background-subtracted) of 47 ± 7 counts (in 0.45−7 keV energy range) are detected.

The bulk of the Chandra Trail counts is found above 0.8 keV. Figure 2 (right panel) shows the very hard nature of the Trail emission. Although the small number of photons hampers a precise charachterization of the Chandra Trail emission parameters, we used the maximum likelihood method implemented in Sherpa with the CSTAT statistic (Cash 1979) to fit the spectrum with an absorbed power law model, fixing the $N_{\rm H}$ to the value derived from X-ray fits of the Geminga pulsar spectrum ($N_{\rm H} = 1.1 \times 10^{20}$ cm^{-2}). The model describes well the data (the Q value – namely, the probability to observe the measured CSTAT statistics or higher if the model is true – is 0.65) and yields $\Gamma = 1.1^{+0.3}_{-0.2}$ (1σ). Such a range is compatible with (if somewhat harder) the photon index seen for the XMM Tails. The observed Chandra Trail flux in the 0.45−7 keV range is $\sim 2.3 \times 10^{-14}$ erg cm^{-2} s^{-1}. We note that the Chandra Trail contributes ∼7% of the Geminga non-thermal flux as measured by XMM-Newton (Caraveo et al. 2004; De Luca et al. 2005), implying that the actual Geminga pulsed fraction above 2 keV is slightly higher than previously reported. However, the correction is smaller than the statistical error on the high energy pulsed fraction quoted by De Luca et al. (2005). In the 0.3−5 keV range, the Chandra Trail has a surface brightness of $\sim 4 \times 10^{-13}$ erg cm^{-2} s^{-1} arcmin^{-2}, i.e. ∼40 times higher than the XMM Tails' one. The unabsorbed flux from the Chandra Trail corresponds to a luminosity of $\sim 5.2 \times 10^{28}$ erg s^{-1}, which is very similar to the estimated XMM Tails' energetic. Thus, the fraction of the pulsar $\dot{E}_{\rm rot}$ converted into X-ray radiation in the arcsec Chandra Trail and in the arcmin XMM Tails is comparable.

The limited FOV of the Chandra observation hampers a direct comparison between Chandra and XMM datasets.

However it is worth noting that in the immediate surrounding of the INS the sensitivity reached by the short Chandra observation would not allow the detection of a diffuse emission as faint as the XMM Tails. Indeed, we estimate the Chandra upper limit for diffuse emission at a level of $\sim 10^{-13}$ erg cm^{-2} s^{-1} arcmin^{-2} (0.45−7 keV, using a $22'' \times 7''$ region), corresponding to a flux 10 times higher than that reported for the XMM Tails. Thus, additional diffuse emission with a surface brightness up to 10 times the value detected by XMM-Newton could easily hide in the Chandra data, making it difficult to obtain a complete picture of the structures around Geminga.

3. Discussion

While the Chandra observation is both too short and with a FOV too limited to shed light on the nature of the XMM Tails, it has added yet another piece to the puzzle of Geminga. A bright, 25″–long trail of hard X-ray emission is now clearly seen behind the pulsar, well aligned with the proper motion direction.

Thus, Geminga joins a small handful of pulsars sporting elongated, "cometary" X-ray diffuse structures, such as, e.g., the Mouse (PSR J1747-2958, Gaensler et al. 2004), the Duck (PSR B1757-24, Kaspi et al. 2001; Gvaramadze 2004), the Black Widow (PSR B1957+20, Stappers et al. 2003) and PSR B1951+32 (Li et al. 2005) which have all been interpreted within a pulsar bow-shock scenario.

Although similar to the case of PSR B1951+32 (embedded in the complex morphology of the SNR CTB 80, Li et al. 2005), the Geminga X-ray emission has a unique symmetry around the pulsar direction of motion. Indeed, the overall morphology of the diffuse features surrounding Geminga, with the small Chandra Trail inside the boundaries of the larger, arc-shaped XMM Tails, is reminiscent of the composite H_α/X-ray nebula associated to the Black Widow. Such nebula is quoted as the most spectacular (and so far unique) confirmation of recent bow-shock theory (e.g. Bucciantini 2002; van der Swaluw et al. 2003; Gaensler et al. 2004; Bucciantini et al. 2005), reflecting the double shock nature of the interaction of a fast moving neutron star with the ISM. An outer arc of H_α radiation is seen, tracing the forward shock, the observed emission coming from collisionally excited, shocked ISM; an inner, cometary X-ray feature is also seen, tracing the region closer to the pulsar, where the shocked pulsar wind emits synchrotron radiation. The case of Geminga shows an obvious and striking difference: both the outer, arc-shaped, and the inner, cometary, features are seen in X-rays, with hard, synchrotron-like spectral shapes.

The XMM-Newton Tails were interpreted as a Bow-shock, traced by very energetic ($\sim 10^{14}$ eV) electrons accelerated by the INS, girating and emitting synchrotron radiation in the shock compressed ambient medium magnetic field (Caraveo et al. 2003). Assuming a spherical pulsar wind in a homogeneous ISM and appling a simple three-dimensional bow-shock model (Wilkin 1996) to the XMM data it was possible to provide an estimate of the unresolved forward stand-off angle $\theta_{\rm fw}$, given by the balance between the ram pressure and the wind pressure ($\theta_{\rm fw} \sim 20''-30''$) and to constrain the inclination angle of Geminga proper motion with respect to the plane of sky ($i < 30^\circ$) as well as the total ISM density ($n \sim 0.1$/cm^3). Indeed, if $\theta_{\rm fw} \sim 20''-30''$ the Chandra Trail would be located in the unshocked pulsar wind region, where no strong synchrotron emission is expected (e.g. Gaensler et al. 2004). However, owing to the large uncertainty involved in fitting the bow-shock model profile to the XMM diffuse feature (which is unresolved from the bright pulsar in its whole "forward" portion), the actual value of $\theta_{\rm fw}$ could be lower and the Chandra Trail could still fit in the proposed scenario of pulsar wind confinement. A forward stand-off distance $\theta_{\rm fw}$ of $\sim 10''$ could be marginally consistent with both XMM and Chandra data. While implying a revision of the system parameters (e.g. the density of the ISM would be ~ 0.5 cm^{-3}), such a scenario would allow to interpret the Chandra Trail as the surface of the termination shock (i.e. the inner interface with the unshocked pulsar wind cavity), where the pulsar wind particles are shocked and accelerated, and start emitting synchrotron radiation. The same interpretation was proposed for other examples of cometary X-ray nebulae explained within a bow-shock scenario, e.g. the Tongue of the Mouse (Gaensler et al. 2004) and the nebula trailing PSR B1757-24 (Gvaramadze 2004), which have indeed a similar morphology. The hard spectrum of the Chandra trail ($\Gamma \sim 0.9-1.4$) is consistent, within the large uncertainty, with synchrotron radiation by freshly injected electrons in the slow cooling regime expected by standard shock theory (Chevalier 2000). The overall shape of the termination shock is elongated since the ram pressure, confining the pulsar wind in the forward direction, is larger than the pressure in the direction opposite to the proper motion. As discussed by Gaensler et al. (2004), this is also expected on the basis of detailed simulations of bow-shock systems (e.g. Bucciantini 2002; van der Swaluw et al. 2003; Gaensler et al. 2004; Bucciantini et al. 2005).

Thus, within such an interpretation the Chandra Trail follows the surface of the pulsar wind termination shock, while the XMM-Newton Tails trace the larger scale, limb brightened, interaction of the pulsar wind with the ISM. Such an interaction, resulting in the formation of a bow-shock, could take place either through a direct contact leading to a mixing between the INS wind and the compressed ISM (Caraveo et al. 2003), or through a contact discontinuity between the two shocked media, as expected by recent simulations (Bucciantini 2002; van der Swaluw et al. 2003; Gaensler et al. 2004; Bucciantini et al. 2005). In the latter scenario, the XMM tails could be associated either to the shocked wind region (where electrons of the pulsar wind emit synchrotron radiation), or to the outer region of the shocked ISM, downstream of the bow-shock interface with the unperturbed ISM (i.e., the region which is usually associated to H_α emission in other cases of pulsar bow-shocks). Hard X-ray photons could be produced there via synchrotron emission by energetic electrons of the shocked pulsar wind leaking into such a region, permeated by the interstellar compressed magnetic field, possibly higher than the magnetic field in the shocked wind region.

Totally different scenarios, where the XMM Tails and the Chandra Trail are unrelated, could also be explored. We note that the phenomenology of the Chandra trail is reminiscent of the jet-like collimated structures seen in the case of Vela (Helfand et al. 2001; Pavlov et al. 2003), another example of

nearby INS shining in high energy γ-rays. In particular, the Geminga's Chandra Trail can be compared to the "inner counterjet" of the Vela PSR (Pavlov et al. 2003) in terms of their absolute projected dimensions ($\sim 5 \times 10^{16}$ cm), spectral shape (photon index $\sim$1.2) and efficiency ($L_{\rm X} \sim 10^{-6}\dot{E}_{\rm rot}$). Although the complex features of the Vela PWN still lack a consistent explanation, and their 3D morphology and orientation is far from understood (Pavlov et al. 2003), they clearly show that the assumption of an isotropic wind outflow is not adequate. As in the case of Vela, Geminga's diffuse features are characterized by a definite symmetry along the proper motion direction.

Before drawing conclusions on the morphology of the structures trailing Geminga, we would like to underline that the combined Chandra/XMM-Newton image shown in Fig. 2, however tantalizing, does not provide a complete and unbiased picture of the INS surroundings. We see bright emission next to the INS and faint emission far from it but, owing to instrument characteristics and/or observing time limitations, Fig. 2 lacks sensitivity in the intermediate flux region where additional structures may be present. Only a deep Chandra observation could yield a complete picture of the system morphology, especially in its forward portion, the piece of evidence needed to ultimately understand its physics.

Acknowledgements. XMM-Newton and Chandra data analysis is supported by the Italian Space Agency (ASI). A.D.L. and F.M. acknowledge an ASI fellowship. We thank an anonymous referee for his/her very helpful comments.

References

Bucciantini, N. 2002, A&A, 387, 1066
Bucciantini, N., Amato, E., & Del Zanna, L. 2005, A&A, 434, 189
Burke, B. E., Gregory, J., Bautz, M. W., et al. 1997, IEEE Trans. Electron Devices, 44, 1633
Caraveo, P. A., & Mignani, R. P. 1999, A&A, 344, 367
Caraveo, P. A., Bignami, G. F., Mignani, R. P., & Taff, L. G. 1996, ApJ, 461, L91
Caraveo, P. A., Lattanzi, M. G., Massone, G., et al. 1998, A&A, 329, L1
Caraveo, P. A., De Luca, A., Mignani, R. P., & Bignami, G. F. 2001, ApJ, 561, 930
Caraveo, P. A., Bignami, G. F., De Luca, A., et al. 2003, Science, 301, 1345
Caraveo, P. A., De Luca, A., Mereghetti, S., Pellizzoni, A., & Bignami, G. F. 2004, Science, 305, 376
Cash, W. 1979, ApJ, 228, 939
Chatterjee, S., & Cordes, J. M. 2002, ApJ, 575, 407
Chevalier, R. A. 2000, ApJ, 539, L45
De Luca, A., Caraveo, P. A., Mereghetti, S., Negroni, M., & Bignami, G. F. 2005, ApJ, 623, 1051
Gaensler, B. M. 2005, Adv. Sp. Res., 35, 1116
Gaensler, B. M., van der Swaluw, E., Camilo, F., et al. 2004, ApJ, 616, 383
Gvaramadze, V. V. 2004, A&A, 415, 1073
Helfand, D. J., Gotthelf, E. V., & Halpern, J. P. 2001, ApJ, 556, 380
Kaspi, V. M., Gotthelf, E. V., Gaensler, B. M., & Lyutikov, M. 2001, ApJ, 560, 371
Lai, D., Chernoff, D. F., & Cordes, J. M. 2001, ApJ, 549, 1111
Li, X. H., Lu, F. J., & Li, T. P. 2005, ApJ, 628, 931
Pavlov, G. G., Teter, M. A., Kargaltsev, O., & Sanwal, D. 2003, ApJ, 591, 1157
Slane, P. 2005, Adv. Sp. Res., 35, 1092
Stappers, B. W., Gaensler, B. M., Kaspi, V. M., van der Klis, M., & Lewin, W. H. G. 2003, Science, 299, 1372
van der Swaluw, E., Achterberg, A., Gallant, Y. A., Downes, T. P., & Keppens, R. 2003, A&A, 397, 913
Wilkin, F. P. 1996, ApJ, 459, L31 A&A, 365, L212